ELSEVIER

Chemical Engineering Journal 137 (2008) 550–560

Chemical Engineering Journal

www.elsevier.com/locate/cej

CFD and experimental model studies for water disinfection tanks with low Reynolds number flows

William B. Rauen [a], Binliang Lin [a], Roger A. Falconer [a,*], Edmilson C. Teixeira [b]

[a] *Hydro-environmental Research Centre, School of Engineering, Cardiff University, The Parade, Cardiff CF24 3AA, UK*
[b] *GEARH/DEA/CT/UFES, Av. Fernando Ferrari 845, Campus Universitario Goiabeiras, Vitoria-ES 29060-410, Brazil*

Received 13 February 2007; received in revised form 13 April 2007; accepted 4 May 2007

Abstract

With the aim of optimising the design of water disinfection tanks through numerical model simulations, results are reported herein of refinements made to a computational fluid dynamics (CFD) code, integrated with scaled hydraulics laboratory experiments, of the flow processes in baffled chlorine contact tanks (CCT). Such chemical reactors are typically used in most water treatment systems worldwide to provide the means for disinfecting water supply. New experimental results obtained for key flow features of a physical CCT model have been used to validate the corresponding CFD predictions. The CFD simulations were performed using an improved low Reynolds number k–ε model to account for relatively low turbulence levels, similar to those occurring in the CCT, and which can also be found in other chemical reactors—particularly at the laboratory model scale. Good agreement was obtained between the CFD predictions and the experimentally measured data, with the modified CFD code predicting the size of a typical mixing zone to within 90% accuracy and giving good agreement with the measured turbulence distribution. The CFD modelling concepts validated herein have ideal potential for use in the simulation of mixing processes and the design of water disinfection tanks in the field and at the laboratory scale as well.

Keywords: Simulation and optimisation; Water disinfection tanks; CFD; Flow and mixing processes; Low Reynolds number flows; k–ε models; Acoustic Doppler velocimetry

1. Introduction

The disinfection of drinking water generally takes place in chlorine contact tanks (CCT), which are typically rectangular basins where baffles are introduced in order to increase the length-to-width ratio of the flow. A channel or pipe is normally used as an inlet device and an overflow weir is generally installed at the outlet. A typical CCT can vary considerably in size, from a relatively small unit, such as the 16 m × 7.5 m × 4.8 m Embsay Contact Tank (studied by Teixeira [1]) as part of the water treatment system for a small community in Northern England, to larger units such as the 91 m × 46 m × 2.5 m Elan Contact Tank (studied by Thayanithy [2]) to suffice the much larger population of Birmingham, U.K. The objective of a CCT is 'to maintain the micro-organisms in the effluent stream in intimate contact with the disinfecting chemical for the required period' [3]. Typical contact times of 15–30 min within a CCT generally give sufficient time for the inactivation of most micro-organisms to take place, although some applications may require much longer contact times.

As shown by White [4], historically chlorine has been the world's most widely used disinfectant. Chlorination of drinking waters has become a worldwide practice, since shortly after the chemical was first used as a germicide in the 19th century. Since the discovery in the 1970s of health hazardous chlorination by-products (CBP), other technologies have been developed and applied for disinfection purposes, such as ozonation, ultraviolet radiation and ultrasonics. However, these technologies have not generally replaced chlorine's near universal use, either as the sole disinfectant in a water treatment plant or in conjunction with other technologies.

Reactions between chlorine compounds and micro-organisms are very complex and time-dependent. The ideal performance of a CCT assumes that all water packets pass through the tank with equal residence times, giving rise to an idealised flow pattern known as 'plug flow'. However, since non-idealities invariably occur in practice, a CCT should be designed to avoid short circuiting and should be as near to a plug flow

* Corresponding author. Tel.: +44 2920 874280; fax: +44 2920 874399.
E-mail address: FalconerRA@cf.ac.uk (R.A. Falconer).

1385-8947/$ – see front matter © 2007 Elsevier B.V. All rights reserved.
doi:10.1016/j.cej.2007.05.011

system as is practicable. This is generally achieved through the use of a pipeline, or a serpentine chamber [3]. Occurrence of recirculating flow regions need to be minimised, since they tend to impair a unit's hydraulic efficiency by increasing the overall mixing levels in the flow and, consequently, causing departure of the flow pattern from plug flow. A 3D flow pattern can typically be the single most significant cause for impairment of a CCT's hydraulic efficiency [1]. As in the context of Teixeira's findings, an optimised CCT will generally have a flow field of a primarily 2D horizontal nature, aiming to provide: (i) the maximum level of microbial inactivation, i.e. disinfection efficiency; (ii) the minimum operational costs, e.g. with reagents; and (iii) the minimum level of CBP formation.

Nonetheless, the flow conditions in existing CCTs can be rather complex, with the occurrence of recirculating flow and dead zones, shear and wall generated turbulence, and regions with relatively low flow velocities, such that sophisticated investigative techniques are required to allow detailed assessments of the actual 'flow through' characteristics in CCTs. Such techniques can involve direct velocity field measurements, e.g. by using laser or acoustic anemometry, and/or by the use of numerical models of the flow and mixing processes in CCTs. However, the availability of reliable hydrodynamic data for use in the verification of numerical model predictions is limited. Hence, thorough comparisons of the performance of CCTs against the predictions of complex three-dimensional (3D) CFD codes have only recently been made—although, in general, CFD simulations of these systems have been performed for 15 years or so.

Previous applications of computational fluid dynamics (CFD) models to predict flow and/or mixing processes in CCTs were somewhat limited, since no attempts were made to validate their predictions [5–7]; or by comparisons between CFD model predictions and measured results only being carried out for 'black-box' tracer outputs [8–11]. These studies lacked a validation analysis of the CFD code with hydrodynamic data obtained in relevant operational conditions, which partly explains why discrepancies often arose when predictions of the mixing levels and solute transport processes were considered.

The few published studies that have involved validation of flow parameters, estimated for CCTs, have generally been based on the mean velocity fields measured in two physical modelling studies, i.e. those of Thayanithy [2] and Teixeira [1]. The velocity measurements in these studies were performed using weighed straws as drogues in the former, and two-dimensional (2D) laser Doppler anemometry (LDA) in the latter. The first technique, although having reproduced the main advective flow rather well, could be expected to give limited or no information on nuances of the turbulent flow characteristics. In spite of this limitation, some good agreement was obtained in comparing the measured velocities with numerical model predictions obtained using a 2D depth-integrated (2DH) numerical model by Falconer and Tebbutt [12] and later by Falconer and Liu [13].

Wang and Falconer [14] carried out comparisons of numerical model predictions against the mean velocity fields in the unit assessed experimentally by Teixeira [1]. The scope of their numerical model simulations was also 2DH, although the mean flow field in a significant portion of Teixeira's baffled tank had a pronounced 3D structure, due to its particular inlet configuration. As a consequence of this limitation good agreement with measured results could only be achieved generally for the region of nearly horizontal 2D flow, i.e. in the latter regions of the tank. Difficulties occurred mainly in obtaining an accurate representation of the mixing zones, in terms of their location, size, and intensity. With regards to the latter, better results were obtained by Wang and Falconer using the standard k–ε model than when the mixing length or large eddy simulation approaches were adopted.

Khan et al. [15] carried out a 3D numerical model simulation of Teixeira's tank and a validation analysis was made of the predicted mean velocity fields and tracer curves. A commercially available CFD package and the standard k–ε model were used. In spite of relatively good agreement being obtained generally for the 3D mean velocity field, their numerical model simulations failed to resolve '(velocity) profiles with multiple inflection points', e.g. those involving some mixing regions.

Shiono and Teixeira [16] provided results of the distribution of turbulence parameters measured in the model CCT investigated by Teixeira [1]. In spite of the provision of their data, no published studies have been found involving the validation of numerical model results for the distribution of turbulence parameters in CCTs. It may be noted that the key CFD model parameter distributions for use in solute transport/mixing simulations are (i) the mean velocity field, and (ii) the turbulence distribution in the simulated tank. A good prediction of the turbulence mixing levels in simulated CCTs can also be used to achieve an optimal mixing strategy for the chemical reactants, by allowing, e.g. the identification of potential regions for enhanced mixing conditions within the tank [17].

In the context of the above there appears to be no consensus as to which numerical modelling tools or approaches should be applied to simulate a wider range of flow conditions, including those typically found in bench scale reactor models, which tend to operate in a different flow regime to those of the corresponding full scale units. It is known that different numerical schemes can give significantly different predictions of the same problem, let alone when certain key parameters are varied. Hence, future design and optimisation studies of water treatment tanks – and potentially other types of chemical reactors – could greatly benefit from the availability of a validated and (to some extent) universal approach to treating the flow processes (including the turbulence characteristics).

The present study addresses the issues highlighted above by further investigating key flow processes that occur in a typical baffled CCT where the flow is primarily two-dimensional, and by identifying, implementing and testing a more suitable CFD modelling approach to simulate such chemical reactors.

2. Experimentation work

Laboratory data acquisition was carried out in a model chlorine contact tank (CCT). The experimentation unit had similar design characteristics to a field-scale CCT, namely the Embsay CCT operated by Yorkshire Water plc. in Northern England. The

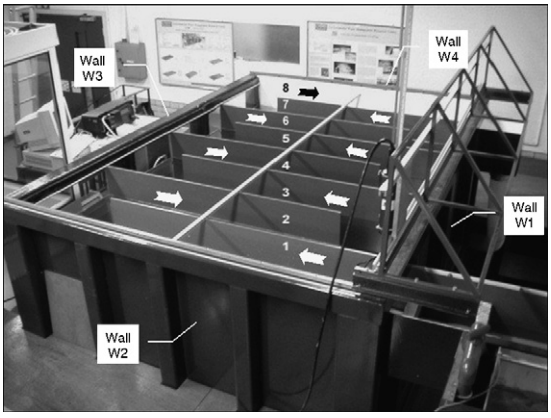

Fig. 1. Laboratory study tank with eight compartments, with the main streamwise flow direction being indicated by arrows.

dimensions of the model tank were 3.0 m long, 2.0 m wide and 1.2 m deep. Baffles made of 12 mm thick PVC sheets were used to produce the baffled configuration, with eight compartments being considered, as shown in Fig. 1, and with each compartment width being $L = 0.365$ m. The main structure of the tank was fabricated in steel and the lateral walls were partially made of glass to allow for flow visualisation. A schematic representation of the model unit in the 2D horizontal plane is shown in Fig. 2a.

An open channel inlet device was connected to compartment 1 at wall W1 of the tank, as shown in the front view of Fig. 2b. The outlet device used was a rectangular sharp-crested weir, located at the end of compartment 8 along wall W1. The experimentation tank was connected to a hydraulic circuit that included two water supply tanks, two centrifugal pumps, an electromagnetic flow meter, and plastic piping and connections.

A series of experiments was conducted in the prototype tank using the channel inlet device and a flow rate of $Q = 3.70$ l/s. This flow rate gave a net mean cross-sectional velocity in the compartments of $U_0 = 10$ mm/s, while the recorded water level in the tank was $H = 1.0$ m. A transient flow regime occurred in the region of uniform 2D flow in the tank, as indicated by the Reynolds number value of around $Re \approx 6000$ calculated as $Re = U_0 4R_h/\nu_l$, where R_h is the hydraulic radius and ν_l is the kinematic viscosity of water.

A 3D acoustic Doppler velocimeter (ADV), manufactured by Nortek, was used to acquire a 3 min long velocity series, at 25 Hz, thus giving 4500 velocity samples at each monitored point. An ADV assessment grid was designed which contained 260 points in a region of nearly 2D horizontal flow and was located at mid-depth, as represented by the shaded area shown in Fig. 2a. A commercially available, neutrally buoyant seeding material normally used in ADV assessments, i.e. Sphericel-110P8, was added in solution to the inflow of the model tank, at approximately 2 h intervals during the ADV measurements. The frequency and amount of seeding material added were controlled so as to maintain the signal-to-noise ratio (SNR) of the acoustic measurements above 15 db and, hence, to improve the reliability of the acquired ADV data [18]. Proper care has been taken with regard to dissolving and adding the seeding material using the water recirculating in the supply system to the model tank, to avoid creating abnormalities in the flow field. The data were processed using the software WinADV [19], thereby providing the desired flow statistics for subsequent analysis. The ADV results are presented and discussed later.

3. CFD modelling

A 3D computational fluid dynamics (CFD) code was developed for simulating the flow processes in water disinfection tanks, using refined equations for low Reynolds number flows and appropriate numerical schemes for high resolution and accuracy. The modelling procedure involved the calculation of a steady-state flow field for inputs of flow rate and water elevations

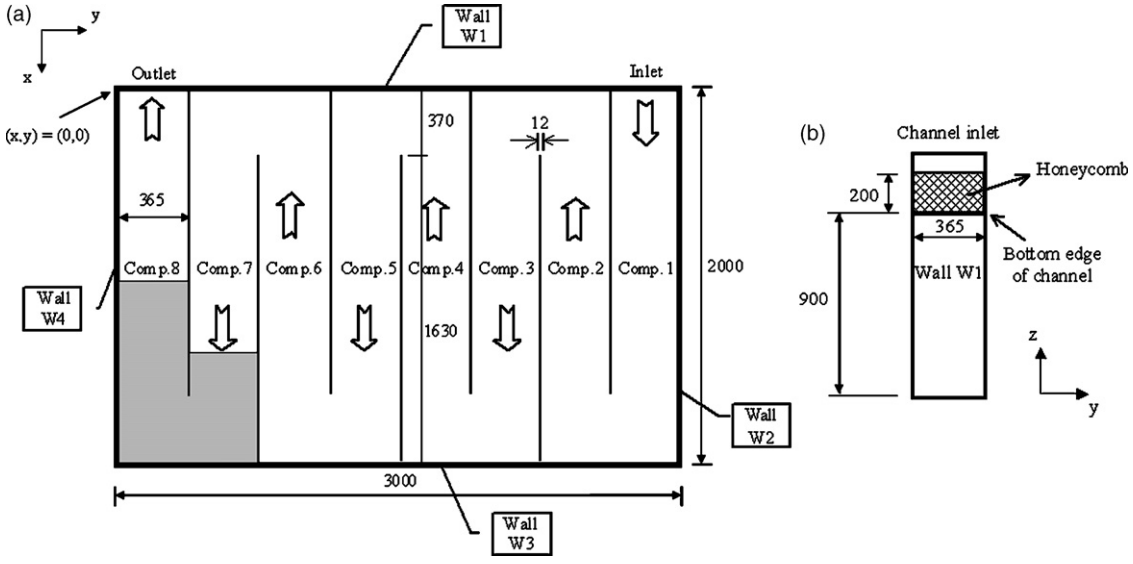

Fig. 2. (a) Schematic plan view of the laboratory tank. The direction of the main streamwise flow in compartments is indicated by the ribbon arrows, while the shaded area represents the region of 2D horizontal flow where the ADV data were recorded; (b) front view of the inlet section, located in compartment 1 of the tank (dimensions in mm).

across the domain. A non-uniform computational grid represented the exact physical domain, with a set of user-specified mesh characteristics enabling the finest and coarsest grid spacings to be setup in each coordinate direction and with the gradient of the mesh being refined near solid boundaries. The inlet and outlet sections and baffles were appropriately located at the pre-processing stage and the domain was mapped to identify the wet, dry, surface, inlet and outlet cells. The fluid properties and other key parameters were then specified for the generation of input files for the flow simulations. The numerical model could be used to simulate either a fully 3D (non-hydrostatic) or a 2D horizontal flow scenario. After a converged solution was obtained with the main solver then a post-processor module was used to generate the computed distributions of the mean velocity and turbulence, which were key outputs for subsequent simulations of the solute transport and mixing processes. The governing equations and further details of the numerical scheme are given below.

The mathematical framework for the main solver of the CFD code involved the fully 3D continuity and momentum (Navier–Stokes) equations for incompressible flow, as well as a low Reynolds number k–ε turbulence model (LReM), where k and ε are the turbulent kinetic energy and dissipation rates, respectively. The LReM proposed by Lam and Bremhorst [20] was used for the turbulence closure model and, hence, two further transport equations were included to account for k and ε variations. The continuity equation expressed in its primitive-variable form and using Cartesian-tensor notation is given as

$$\frac{\partial U_i}{\partial x_i} = 0 \tag{1}$$

while the transport equation can be expressed in general form as

$$U_j \frac{\partial \phi}{\partial x_j} = \frac{\partial}{\partial x_i}\left(D \frac{\partial \phi}{\partial x_j}\right) + S \tag{2}$$

where $i, j = 1, 2, 3$ correspond to the x, y and z directions, respectively; U_i or U_j is the mean velocity in the x_i or x_j direction; ν_l is the kinematic viscosity; and the terms ϕ, D and S are specified according to Table 1 for each type of transport equation. Further parameters involved in the governing equations included: ν_t as the eddy viscosity, given by Eq. (3); ρ the fluid density; P the pressure; and G as the turbulence generation term given by Eq. (4):

$$\nu_t = c_\mu f_\mu \frac{k^2}{\varepsilon} \tag{3}$$

Table 1
Specification of the variables in the general transport equation (2)

Equation	Term		
	ϕ: dependent variable	D: diffusion coefficient	S: source-term
Momentum	U_i	$\nu_l + \nu_t$	$-\frac{1}{\rho}\frac{\partial P}{\partial x_i}$
Turbulent kinetic energy	k	$\nu_l + \frac{\nu_t}{\sigma_k}$	$G - \varepsilon$
Dissipation rate	ε	$\nu_l + \frac{\nu_t}{\sigma_\varepsilon}$	$f_1 c_{1\varepsilon}\frac{\varepsilon}{k}G - f_2 c_{2\varepsilon}\frac{\varepsilon^2}{k}$

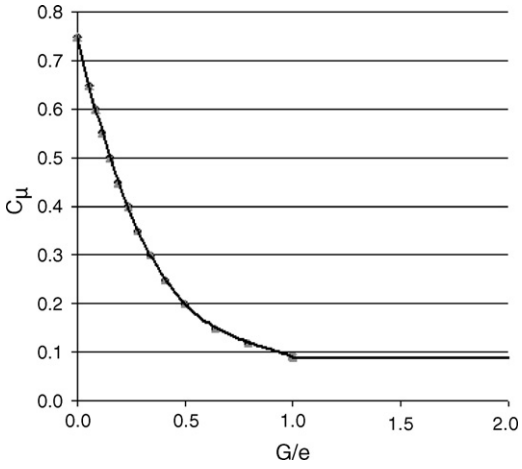

Fig. 3. Determination of the c_μ parameter for the LB model as a function of the ratio of local turbulence generation to the dissipation rate (G/ε), adapted from Rodi [21].

$$G = \nu_t \frac{\partial U_i}{\partial x_j}\left(\frac{\partial U_i}{\partial x_j} + \frac{\partial U_j}{\partial x_i}\right) \tag{4}$$

The values of the turbulence model constants σ_k, σ_ε, $c_{1\varepsilon}$ and $c_{2\varepsilon}$ were 1.44, 1.92, 1.0 and 1.3, respectively [20,21]. Two approaches were used to calculate c_μ for use in Eq. (3), namely: (i) as a constant parameter, where $c_\mu = 0.09$, i.e. as it is generally used in k–ε model simulations [21] and (ii) as a function of the local degree of strain in the flow, where $c_\mu = f(G/\varepsilon)$, as illustrated in Fig. 3, following an empirical formulation originally proposed by Rodi [22]. Where $G/\varepsilon > 1.0$ then c_μ was made equal to 0.09 to reflect its general form of use. A best-fit polynomial regression function with $R^2 = 0.99$ has been derived in this study for use in the numerical model in calculations of the c_μ variation in the interval $0.0 < G/\varepsilon \leq 1.0$, which reads:

$$c_\mu = -0.82\left(\frac{G}{\varepsilon}\right)^3 + 2.11\left(\frac{G}{\varepsilon}\right)^2 - 1.95\left(\frac{G}{\varepsilon}\right) + 0.75 \quad \text{for } 0.0 < \frac{G}{\varepsilon} \leq 1.0 \tag{5}$$

This function had a maximum value of $c_\mu = 0.75$ for $G/\varepsilon = 0.0$, and a minimum value of $c_\mu = 0.09$ for $G/\varepsilon = 1.0$, which typically occurred around $y^+ \approx 10$ in the numerical model simulations of the present study. The results obtained with the two c_μ modelling approaches have been compared with published data and it has been found that the variable c_μ approach gave improved predictions of the characteristic mean velocity profile of the near wall region for both the transient and turbulent flow regimes, as shown later.

Inclusion of the damping function f_μ in Eq. (3) and f_1 and f_2 in the source-term of the ε equation (see Table 1) was due to the use of an LReM. Unlike f_μ, the damping functions f_1 and f_2 had only an indirect effect on the calculation of the eddy viscosity, by affecting the computation of the ε distribution across the flow field. In the Lam and Bremhorst model these functions are

calculated as follows:

$$f_\mu = (1 - e^{-0.0165R_y})^2 \left(1 + \frac{20.5}{R_T}\right) \quad (6)$$

$$f_1 = 1 + \left(\frac{0.05}{f_\mu}\right)^3 \quad (7)$$

$$f_2 = 1 - e^{-R_T^2} \quad (8)$$

where R_y and R_T are the turbulence Reynolds numbers, which are obtained using:

$$R_y = \frac{y\sqrt{k}}{\nu_l} \quad (9)$$

$$R_T = \frac{k^2}{\varepsilon \nu_l} \quad (10)$$

where y is the normal distance from a grid point to the nearest solid boundary. For fully turbulent flows the value assumed by the damping functions tends to unity in the region away from solid boundaries [23]. Hence, the turbulence model transport equations become similar to those of the standard k–ε model in these regions. A constraint was imposed for the minimum value assumed by f_μ and f_2 to avoid spurious numerical oscillations, particularly in the near wall region, so that $f_\mu, f_2 > 0.01$.

Generally in using an LReM approach the computational grid must be refined near solid boundaries, since a relatively high mesh resolution is required for an accurate computation of the locally steep gradients of the flow quantities. In this study the first grid point near a wall boundary would be located typically at $y^+ < 1$, while at least five grid points would be placed within the region of $y^+ < 10$, where $y^+ = yu_f/\nu_l$ is the dimensionless wall distance and u_f is the friction velocity.

The prescription of the boundary conditions for the governing equations followed the definitions of Roache [24] and the work of Stamou [10]. These included: the no-slip/no-flux condition at solid boundaries; the rigid-lid with a free slip assumption for representing the free surface in a 3D problem; and the Neumann and Dirichlet boundary conditions applied, respectively to the outlet and inlet sections of the simulated domain. The prescription of wall boundary conditions for the LReM involved setting $k = 0$ at the wall and using the Neumann condition for ε [23]. At the free surface the Neumann and Dirichlet boundary conditions were used for k and ε, respectively.

The governing equations were discretised using the finite volume method and a staggered-mesh approach. The iterative SIMPLER algorithm of Patankar [25] was used to solve the velocity–pressure link of the momentum equations. The resulting sets of discretised equations were solved using a semi-implicit, line-by-line technique, in which a tridiagonal system of equations were solved for in alternating sweeps along the coordinate directions of the computational domain. This solution process was performed throughout the computational domain until a converged velocity field solution was obtained, which was governed by the ratio between the outflow and inflow rates in terms of establishing flow convergence. This implied that the solution process would be deemed complete when the ratio of the outflow to the inflow became asymptotic to unity. Further details of the CFD code used are provided in Rauen [26].

4. Variable c_μ approach for modelling near wall flows

The appropriateness of incorporating the variable c_μ modelling approach into the LReM, as described by Eq. (5), was assessed from comparisons with available near wall data. In Fig. 4 the numerical model results obtained for the variation of the $c_\mu f_\mu$ product, with the dimensionless wall distance y^+, were compared with the f_μ data of Patel et al. [23] multiplied by $c_\mu = 0.09$. The numerical model results were taken within the fully developed region of a wide 2D horizontal channel.

It can be noted from Fig. 4 that a better estimate of the $c_\mu f_\mu$ curve was obtained when using the variable c_μ approach, in comparison with using the value of $c_\mu = 0.09$ in the region of $y^+ < 10$ approximately, i.e. the laminar sub-layer of the near wall zone. For y^+ values greater than about 10 (approximately), then the two computed distributions were practically coincident and with excellent agreement being obtained between both sets of data for values in the range $10 < y^+ < 40$ (approximately). For values of $y^+ > 40$ then the calculated values for $c_\mu f_\mu$ were generally lower than the corresponding empirical results, with the distributions becoming asymptotic to $c_\mu f_\mu \approx 0.09$ for $y^+ \approx 120$–130, whilst from the data the asymptote occurred at $y^+ \approx 80$–90. As discussed by Patel et al. [23] this behaviour is characteristic of the turbulence model used, i.e. the LReM of Lam and Bremhorst [20].

Two related aspects should be highlighted with regard to the above results. Firstly, in using the variable c_μ approach the computed c_μ values reached the asymptote of 0.09 for $y^+ \approx 10$ (approximately). Thus, the computed $c_\mu f_\mu$ distributions became asymptotic at 0.09 as f_μ tended to unity, i.e. towards the fully turbulent layer of the near wall zone. Secondly, the damping functions f_1 and f_2 typically reached unity nearer the wall than f_μ, e.g. around $y^+ \approx 30$–40 for f_1 and $y^+ \approx 2$–5 for f_2. Hence, for y^+ values higher than about 120–130, the numerical model simulations were essentially performed using the standard k–ε model formulation, since $f_\mu = f_1 = f_2 = 1$ in the outer region.

The improved $c_\mu f_\mu$ results that were obtained with the variable c_μ approach can be expected to have a direct beneficial effect on predictions of the eddy viscosity distribution calculated with Eq. (3) and, consequently, on the velocity profiles. These

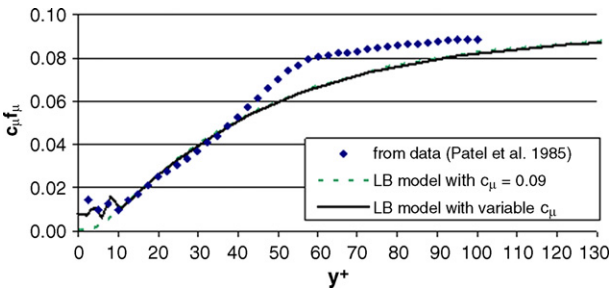

Fig. 4. Variation of the $c_\mu f_\mu$ product with the dimensionless wall distance y^+ (LB model stands for the low Reynolds number k–ε turbulence model of Lam and Bremhorst [20] and c_μ represents the c_μ parameter of the turbulence model).

effects were verified by comparing the near wall velocity profiles calculated using the variable and constant c_μ approaches, with the typical velocity distributions that occurred in the vicinity of a smooth wall, given by Boyer and Laurence [27] as

$$U^+ = \frac{1}{\kappa}\ln(1+0.41y^+) + 7.8\left(1 - e^{-(y^+/11)} - \frac{y^+}{11}e^{-(y^+/3)}\right) \quad (11)$$

where $\kappa = 0.4187$ is the von Kármán constant and $U^+ = U/u_f$ is the normalised velocity.

Comparisons of Eq. (11) with the near wall velocity profiles obtained with the numerical model using the constant and variable c_μ approaches are shown in Fig. 5. The transient and turbulent flow regimes were simulated for Reynolds numbers of $Re = 5000$ and 30,000 respectively. These simulations were undertaken to check the consistency of the numerical model results, since the near wall velocity distribution is independent of the Reynolds number. The results in Fig. 5 have confirmed that a more accurate prediction of the velocity profile was obtained when the variable c_μ approach was used as part of the LReM simulations, as proposed in this study, for both flow regimes. These results also showed that better agreement with the near wall velocity distribution occurred generally for $y^+ > 10$, in spite of the fact that improvements in the $c_\mu f_\mu$ curve calculated using the variable c_μ approach were obtained for $y^+ < 10$. This finding seemed to stress the importance of accurately predicting the near wall flow features when using an LReM formulation. Promoting an increased resolution of the computational grid in such flow regions is crucial, but the verification results discussed herein showed that the modification made to the c_μ formulation in the turbulence model led to further improvements in the CFD predictions.

5. Physical experimentation results

The time velocity series measured by the ADV in the prototype tank were used to calculate the mean velocity field and the distribution of the Reynolds stresses for the assessed velocity cross-sections. These ADV measurements were carried out in a region of nearly 2D horizontal flow, as indicated by the shaded area in Fig. 2a. As verified experimentally by Rauen [26] this region was virtually free from the 3D flow effects caused by the inlet configuration and was selected as representative of a typical vertically uniform flow around a 180° bend in a baffled CCT.

The mean resultant velocity field (R) measured by the ADV in the model tank and the corresponding streamtrace plot are shown in Fig. 6a. The coordinate system dimensions have been normalised by the compartment width (L), with the mean resultant velocity being normalised by the mean cross-sectional velocity (U_0) in these and subsequent figures. It can be noted from Fig. 6a that a horizontally reversed flow structure occurred at the upstream portion of compartment 8, alongside the baffle separating compartments 7 and 8. This zone is represented schematically in Fig. 6d as 'zone A'. This type of flow structure occurs typically in baffled CCTs due to flow deflection by the tank walls, concurrently with flow separation in the baffle lee [1]. The measured results indicated that the length and width of the recirculation zone were approximately $1.4L$ and $0.4L$, respectively.

The results of Fig. 6a were further used to identify the location of the main advective flow path in the assessed cross-section, which was found to occupy the region represented as 'zone B' in Fig. 6d. This region corresponded to locations where the resultant mean velocity was equal to, or higher than, U_0, i.e. where $R/U_0 \geq 1.0$ as can be depicted from Fig. 6e. Further analysis of these results indicated that the advective flow path occupied around 45% of the assessed cross-section. It is worth of notice that Fig. 6 also includes results from the numerical model simulations for comparison, which are discussed in the following section.

The normalised distribution of the Reynolds stresses obtained from the ADV data is shown in Fig. 6a. The Reynolds stresses were calculated as the ratio of the covariance of the horizontal velocity components to the product of the standard deviations of each time velocity series [28]. Normalisation using the maximum occurring value was then performed, followed

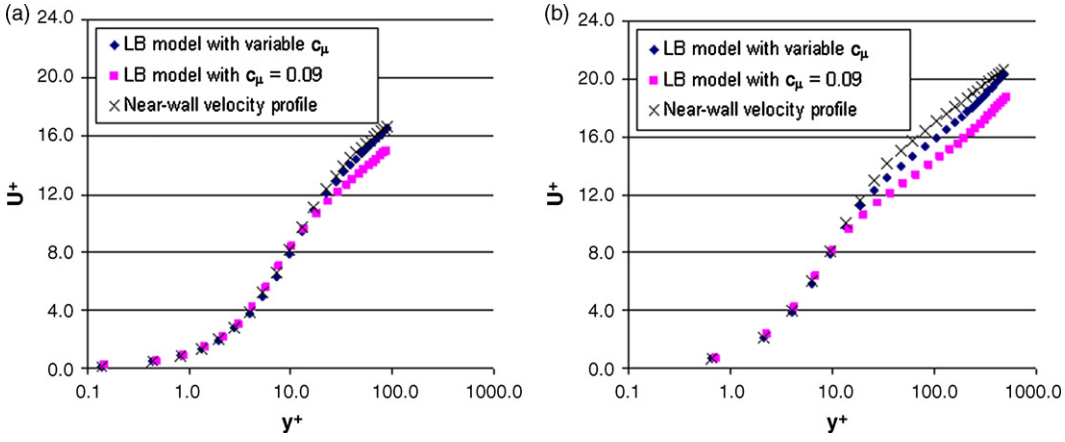

Fig. 5. Comparison between the near wall velocity profile and CFD results for: (a) $Re = 5000$ and (b) $Re = 30{,}000$ (LB model stands for the low Reynolds number k–ε turbulence model of Lam and Bremhorst [20] and c_μ represents the c_μ parameter of the turbulence model).

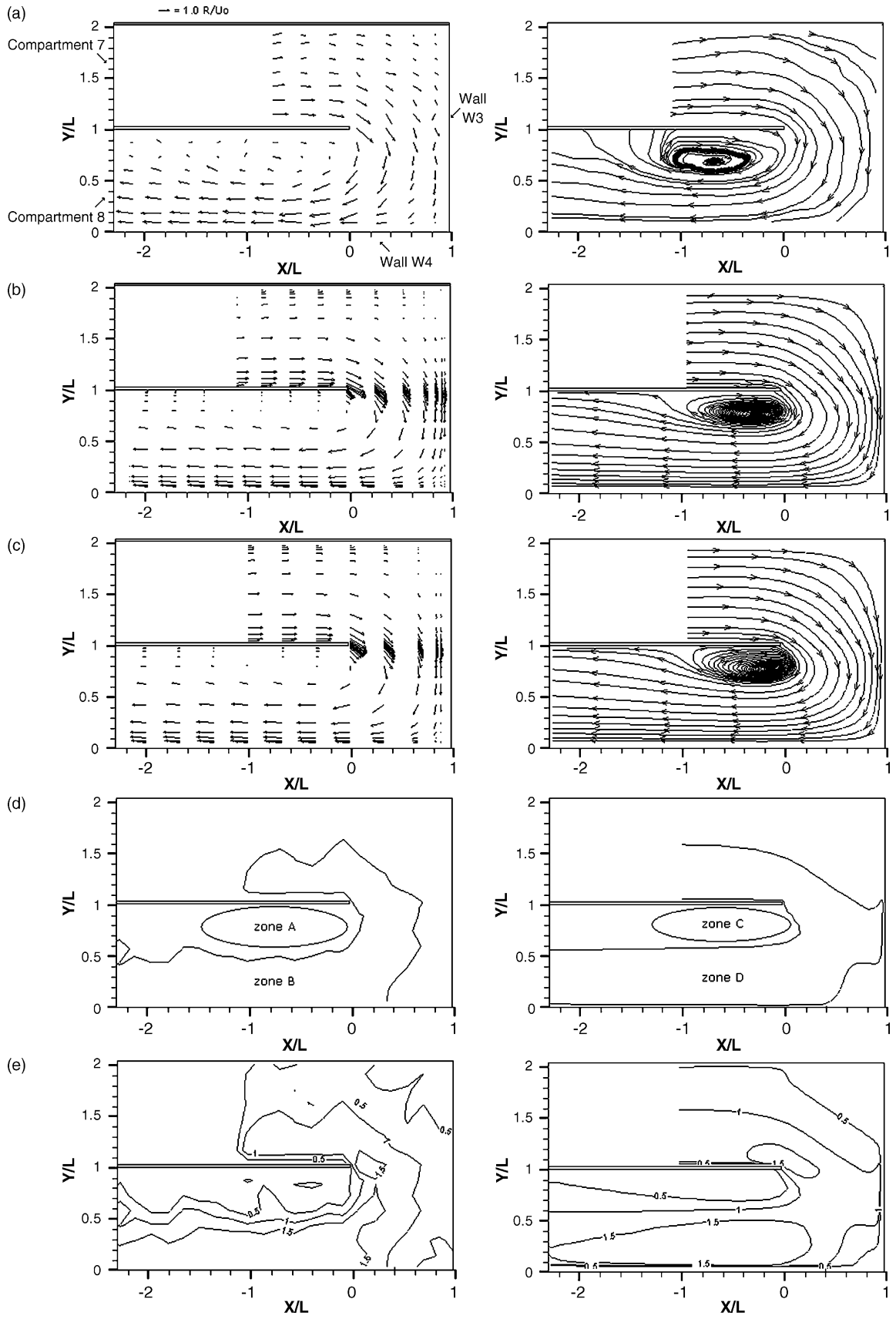

Fig. 6. Normalised mean velocity field (R/U_0) and corresponding streamtraces in the bend between compartments 7 and 8 of the laboratory tank, showing (a) experimental results; (b) numerical model results for mesh 'M1'; (c) numerical model results for mesh 'M2'; (d) identification of zones of interest; (e) isovels for the experimental and numerical model results for mesh 'M2', respectively.

by extraction of the cubic root of these results to allow for a better visualisation of even relatively low values obtained from the measured data. It can be seen from Fig. 6a that local maxima of the normalised Reynolds stresses occurred in zones 'uv1' and 'uv3', as illustrated in Fig. 6b. These zones were generally located near the edges of the main advective flow path (as identified in Fig. 6b) owing to the relatively high velocity gradients occurring between 'zone B' and the surrounding flow.

6. CFD simulations of the model tank—discussion

Numerical model simulations of the model CCT were carried out using two computational grid configurations to verify the independence of the solutions. Meshes 'M1' and 'M2' of a rectangular, non-uniform computational grid that fitted exactly the dimensions of the experimentation unit were constructed, as illustrated in Fig. 7. The grid spacings of mesh 'M1' varied from 1 mm near the tank walls and baffles to 50 mm towards the centre of the compartments, giving 51 cells in the x direction and 239 cells in the y direction. The mesh 'M2' had a finer grid spacing, with nearly twice the total number of grid points, with the corresponding mesh spacings being in the range from 1 mm to 30 mm, giving 84 cells and 290 cells in the x and y directions, respectively. Computations with coarser grids were only performed during the preliminary testing stages of the CFD model and in order to assess if mass conservative solutions were being generated. The accuracy of the results obtained was not verified, since proper care had not been taken at that stage to design the computational grid with an adequate resolution, particularly near the walls. For this reason, such results were not included in the paper. Furthermore, due to the complexity of the flow field in water disinfection tanks the optimisation of the computational grid for CFD simulations of such reactors can be a very demanding and time consuming task in itself. Therefore, this task was not attempted in this study after grid independence was verified for meshes 'M1' and 'M2'.

The numerical model simulations were set up to reproduce the experimentation conditions described previously. The results for the mean velocity field and the streamtraces, obtained using meshes 'M1' and 'M2', are shown in Fig. 6b and c, respectively. The corresponding results for the normalised Reynolds stress distributions are shown in Fig. 8c and d, respectively. The computational time for obtaining a converged flow field solution with mesh 'M1' was approximately 90 min on a Pentium 4, 1.7 GHz with 512 MB RAM computer.

In Fig. 6b and c it can be seen that the occurrence of a mixing zone at the upstream region of compartment 8, alongside the baffle, was predicted by the CFD code in a similar manner using both mesh configurations. Furthermore, in the computed results this zone occurred at approximately the same location as verified in the measured results of Fig. 6a. The mixing zones obtained with the two mesh configurations were similar in size, with the length and width corresponding to $1.3L$ and $0.35L$, respectively (illustrated as 'zone C' in Fig. 6d). In comparison with the corresponding data these computed results showed an underestimation of the velocities to within an order of 10%. The main advective flow path predicted by the numerical model is shown in Fig. 6d as 'zone D'. This region occupied approximately 50% of the cross section area, with this result being in close agreement with the corresponding measurements discussed earlier. It can be noted from Fig. 6e that the agreement between the empirical and computed isovels was also very good,

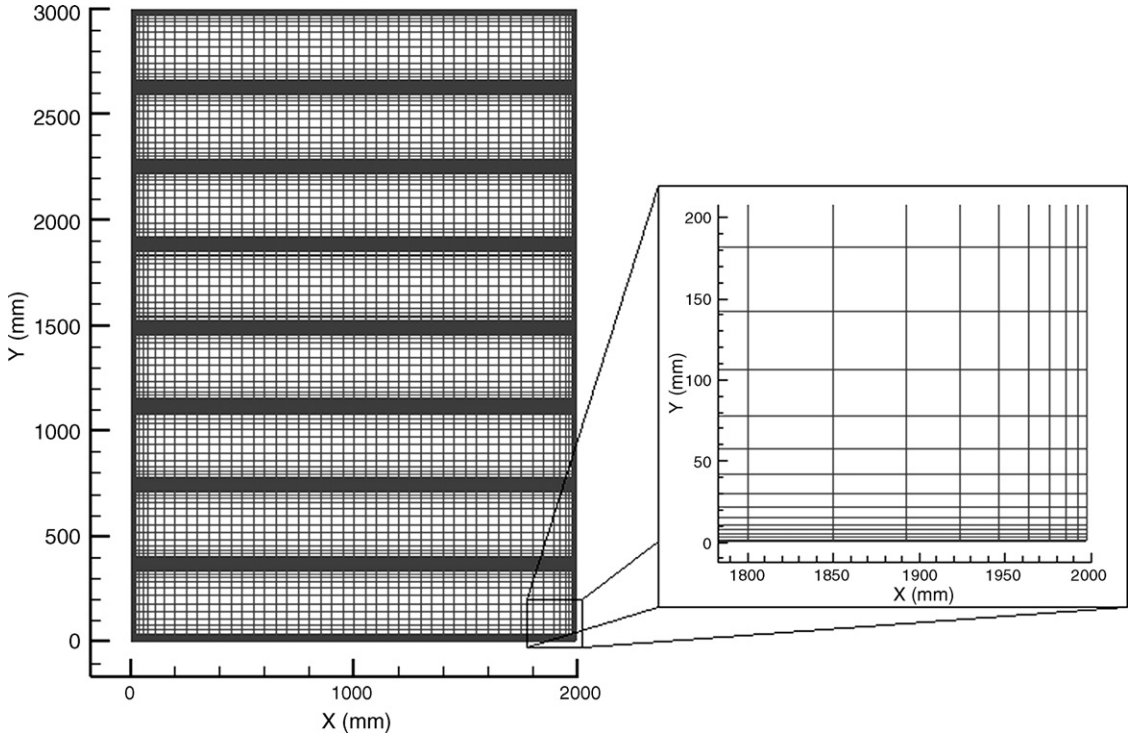

Fig. 7. Computational mesh 'M1' as used in the numerical model simulations of the laboratory tank.

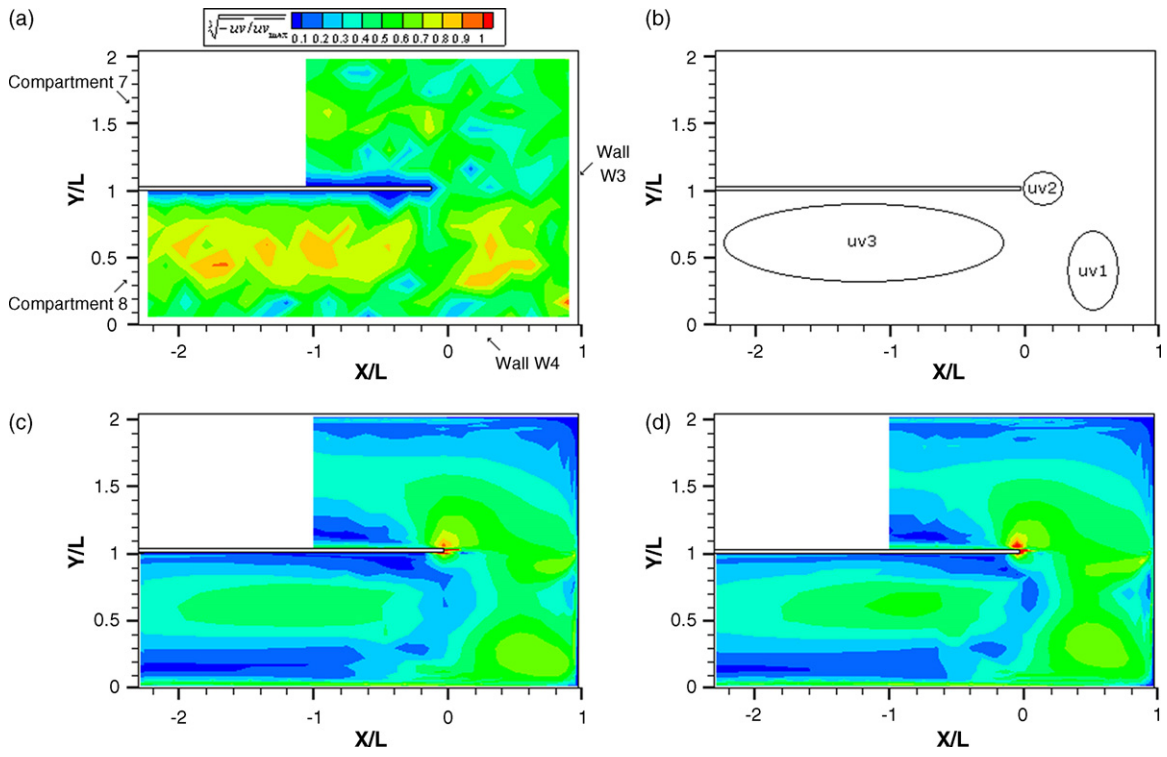

Fig. 8. Isocontours of the normalised Reynolds stress term, showing (a) experimental results; (b) identification of zones of interest; (c) numerical model results for mesh 'M1'; and (d) numerical model results for mesh 'M2'.

except for a relatively small area along wall W3. Analysis of the computed distributions of the Reynolds stress term offered a possible explanation for such a discrepancy, as discussed below.

The Reynolds stresses were calculated from the numerical model results using the Boussinesq assumption, with these results being subsequently normalised in a similar manner as for the experimental results. The normalised Reynolds stress distributions were obtained using meshes 'M1' and 'M2' and the predictions are shown in Fig. 8c and d, respectively. An analysis of these results indicated that local maxima of the Reynolds stresses were correctly predicted to occur around regions 'uv1' and 'uv3' of the cross section, as indicated in Fig. 6b, with good agreement between the predicted and measured results also being obtained elsewhere across the domain. An exception was the region in front of the baffle lee, i.e. zone 'uv2', where the numerical model unduly predicted relatively high levels of the Reynolds stresses. Since zone 'uv2' was situated in the main advective flow path of this flow cross section, as illustrated in Fig. 6d, this may have impaired the prediction of the advective levels further downstream of this location, e.g. in the region of advective flow along the wall W3. The possible causes of this mismatch are currently being investigated further, but at the time of this study this anomaly was deemed not to affect significantly the numerical model results.

The key strengths of a CFD modelling approach using an LReM can be seen as the drawbacks of the more traditional approach using the standard k–ε turbulence model. The use of such model in CFD simulations for complex flows should be made with care, since the accuracy of the predictions is typically reduced near separation and reattachment points, and in regions where the flow field is not highly turbulent [21]. The literature show that these conditions can be found in water disinfection tanks at the prototype scale and also at the field scale [16], specially when the flow pattern deviates largely from plug flow.

The expected effects of applying the standard k–ε model – as opposed to an LReM – in CFD simulations of the model tank could have been two-fold. Firstly, a computational grid designed for CFD simulations with the standard k–ε model might not have provided enough resolution for an accurate computation of key flow features, such as the mixing zones in the tank, due to the use of the wall function boundary condition. As a consequence, the computed intensity of the advective flow and the turbulence levels in the modelled tank could also have been affected. This, in turn, could have jeopardised the accuracy of any subsequent computation of, e.g. the residence time distribution (RTD) for the tank—and, hence, the corresponding CFD prediction of the levels of short circuiting and mixing in the flow.

Secondly, since the standard k–ε model has been developed for simulating highly turbulent flows, it has limited use in CFD computations of flows with low to intermediate turbulence levels, such as regions with relatively low flow velocities, dead zones, as well as flow separation and reattachment areas—which are typically associated with the occurrence of recirculation zones in flow reactors. Such conditions can frequently be found in field scale contact tanks requiring hydraulic optimisation, which can have a flow pattern tending to complete mixing and with dead zones occupying large portions of the tank. Non-

highly turbulent flow regimes are also typical at the prototype scale, as shown for the model tank of this study. In such cases, a CFD model equipped with an LReM can be a more appropriate and robust tool for the design and optimisation of the hydraulic behaviour of water disinfection tanks and their prototypes.

Further studies would be required to assess the impact of refined CFD flow field predictions on the simulation results for the solute transport and disinfection processes for CCTs, or other chemical reaction processes. A refined CFD model including an LReM, rather than a more traditional standard k–ε turbulence model, would be expected to provide more accurate estimates of the short circuiting and mixing levels of a flow reactor. However, any such improvements in accuracy have to be balanced by the increase in computational time required to perform the CFD simulations using an LReM approach (typically due to the higher number of grid cells associated with the use of this type of turbulence model). It is worth noting that continuous advances in computing power have made practical 2D LReM simulations an attractive option in recent times, with the 3D case expected to follow.

7. Conclusions

In this study a physical and numerical model investigation of key flow processes in chlorine contact tanks (CCT) has been undertaken. Velocity measurements were carried out in a model CCT using a 3D acoustic Doppler velocimeter (ADV) and the corresponding results were analysed in terms of the mean velocity field and the distribution of the Reynolds stresses. Key features of the flow field in a typical mixing region of the baffled tank were characterised.

A purpose-built computational fluid dynamics (CFD) code was tested in simulations of a baffled CCT. The theoretical range of applicability of the adopted modelling approach spans from full scale units to bench scale hydraulic models, and from laminar to fully turbulent flow regimes, so that the validated CFD model has ideal potential for application in the simulation of a range of water treatment tanks.

A modified version of a low Reynolds number k–ε turbulence model (LReM) was proposed and validated. The modification involved the inclusion of a variable c_μ modelling approach in the original turbulence model equations, where c_μ is a function of the ratio between the local turbulence production and the dissipation levels. It was shown that the modified model gave improved predictions of the $c_\mu f_\mu$ term in the turbulent viscosity equation relative to the original formulation, with a direct beneficial effect on the computed near wall velocity profiles. The adoption of such a variable c_μ approach, as proposed herein, could improve the predictive ability of similar turbulence models used in CFD simulations of various chemical reactors.

The CFD code was applied to simulate the flow processes measured in the laboratory CCT facility. Good agreement was obtained for the assessed flow features, as characterised from the physical experimentation results. The distributions of the normalised Reynolds stresses and the mean advective flow were generally well predicted, while the size and intensity of a typical mixing zone was estimated to around 90% accuracy. Overall the validation analyses of the numerical model results with data from the scaled hydraulic laboratory experiments confirmed the appropriateness of the proposed numerical modelling approach for simulating and optimising the design of typical water disinfection tanks in the field and laboratory scale as well.

Acknowledgment

The first author acknowledges the receipt of a Ph.D. scholarship from CAPES Foundation (Brasilia, Brazil).

References

[1] E.C. Teixeira, Hydrodynamic processes and hydraulic efficiency of chlorine contact units. Ph.D. Thesis, University of Bradford, UK, 1993.
[2] M. Thayanithy, Hydraulic design aspects of chlorine contact tank, M.Sc. Dissertation, University of Birmingham, UK, 1984.
[3] BSI, Wastewater Treatment Plants – Part 14: Disinfection. British Standard BS EN 12255-14 http://www.bsonline.bsi-global.com/server/index.jsp.
[4] G.C. White, Handbook of Chlorination and Alternative Disinfectants, 4th ed., John Wiley & Sons, New York, 1998.
[5] W.M. Grayman, R.A. Deininger, A. Green, P.F. Boulos, R.W. Bowcock, C.C. Godwin, Water quality and mixing models for tanks and reservoirs, J. AWWA 88 (7) (1996) 60–73.
[6] I.A. Hannoun, P.F. Boulos, Optimizing distribution storage water quality: a hydrodynamic approach, Appl. Math. Model. 21 (1997) 495–502.
[7] I.A. Hannoun, P.F. Boulos, E.J. List, Using hydraulic modelling to optimize contact time, J. AWWA 90 (8) (1998) 77–87.
[8] R.A. Falconer, A.I.B.M. Ismail, Numerical modelling of tracer transport in a contact tank, Environ. Int. 23 (6) (1997) 763–773.
[9] D.K. Peplinski, J.J. Ducoste, Modeling of disinfection contactor hydraulics under uncertainty, J. Environ. Eng. ASCE 128 (11) (2002) 1056–1067.
[10] A.I. Stamou, Verification and application of a mathematical model for the assessment of the effect of guiding walls on the hydraulic efficiency of chlorination tanks, J. Hydroinform. 4 (4) (2002) 245–254.
[11] D.J. Greene, B. Farouk, C.N. Haas, CFD design approach for chlorine disinfection processes, J. AWWA 96 (8) (2004) 138–150.
[12] R.A. Falconer, T.H.Y. Tebbutt, A theoretical and hydraulic model study of a chlorine contact tank, Proc. ICE 2 (81) (1986) 255–276.
[13] R.A. Falconer, S.Q. Liu, Modelling solute transport using QUICK scheme, J. Environ. Eng. ASCE 114 (1) (1988) 3–20.
[14] H. Wang, R.A. Falconer, Numerical modelling of flow in chlorine disinfection tanks, J. Hydraul. Eng. ASCE 124 (9) (1998) 918–931.
[15] L.A. Khan, E.A. Wicklein, E.C. Teixeira, Validation of a three-dimensional computational fluid dynamics model of a contact tank, J. Hydraul. Eng. 132 (7) (2006) 741–746.
[16] K. Shiono, E.C. Teixeira, Turbulent characteristics in a baffled contact tank, J. Hydraul. Res. 38 (6) (2000) 403–416.
[17] Y. Liu, J. Ducoste, Numerical simulation of chloramines formation in turbulent flow using a multi-fluid micromixing model, Environ. Model. Softw. 21 (2006) 1198–1213.
[18] S.J. McLelland, A.P. Nicholas, A new method for evaluating errors in high-frequency ADV measurements, Hydrol. Process. 14 (2000) 351–366.
[19] T. Wahl, Analysing ADV data using WinADV, in: Proc. Joint Conf. Water Resour. Eng. Water Res. Plan. Manage., Minneapolis, USA, 2000.
[20] C.K.G. Lam, K. Bremhorst, A modified form of the k–ε model for predicting wall turbulence, J. Fluids Eng. ASME 103 (1981) 456–460.
[21] W. Rodi, Turbulence Models and Their Application in Hydraulics—A State-of-the-Art Review, 3rd ed., A.A. Balkema, Rotterdam/Brookfield, 1993.
[22] W. Rodi, The prediction of free turbulent boundary layers by use of a two-equation model of turbulence, Ph.D. Thesis, University of London, 1972.

[23] V. Patel, W. Rodi, G. Scheuerer, Turbulence models for near-wall and low Reynolds number flows: a review, AIAA J. 23 (9) (1985) 1308–1319.
[24] P.J. Roache, Fundamentals of Computational Fluid Dynamics, Hermosa Publishers, New York, 1998.
[25] S.V. Patankar, Numerical Heat Transfer and Fluid Flow, Hemisphere, New York, 1980.
[26] W.B. Rauen, Physical and numerical modelling of 3-D flow and mixing processes in contact tanks, Ph.D. Thesis, Cardiff University, UK, 2005.
[27] V. Boyer, D. Laurence, A shape function approach for high- and low-Reynolds near-wall turbulence models, Int. J. Numer. Meth. Fluids 40 (2002) 241–251.
[28] J.O. Hinze, Turbulence, 2nd ed., McGraw-Hill, New York, 1975.